RSC Advances

ROYAL SOCIETY OF CHEMISTRY

www.rsc.org/advances

Dendrimer Confined Pt Nanoparticles: Electro-Catalytic Activity towards Oxygen Reduction Reaction and its Application in Polymer Electrolyte Membrane Fuel Cells

A. Arunchander, S. Gouse Peera, V. Parthiban, Srinu Akula, Tintula Kottakkat, Santoshkumar D. Bhat and Akhila Kumar Sahu*

Dendrimers have shown as a promising candidate in controlling size, shape and avoid agglomeration of the metal nanoparticles. Platinum nanoparticles are stabilized by fourth generation amine terminated poly(amidoamine) (G4-PAMAM) dendrimers and anchored successively onto carbon by two methods, namely ester functionalization (Pt-DENs/C_{est}) and active anhydride functionalization (Pt-DENs/C_{anh}) as the cathode catalyst in polymer electrolyte membrane fuel cells (PEMFCs). The effects of pH and reaction time on complexation reaction are examined by UV-vis spectroscopic technique. The electronic and structural features of nanoparticles are studied by X – ray photoelectron spectroscopy (XPS), X – ray diffraction technique (XRD) and Transmission Electron Microscope (TEM). Electrochemical behaviour and catalytic activity of the catalysts are studied by cyclic voltammograms (CV) and linear sweep voltammograms (LSV) in N_2 and O_2 saturated 0.1 M aqueous $HClO_4$. Effect of functionalization is studied and the significant result has observed. PEMFC performance of the catalysts synthesized using dendrimer was compared with the catalyst without dendrimer. Pt-DENs/C_{anh} show significant performance over Pt/C prepared in the absence of dendrimer.

Introduction

Platinum based electrocatalyst is widely used in low-temperature polymer electrolyte membrane fuel cells (PEMFCs) to decrease the voltage loss associated with slow oxygen reduction reaction (ORR) kinetics.[1] Owing to the high cost of Pt catalyst and limitation on global supplies, there is a definite need to reduce the metal loading for PEMFC to be cost-effective. An effective way of reducing the Pt loading without compromising the PEMFC performance is to adapt nano-platinum particulates as catalyst. While doing so, the effects of particle size, quantum size-effects, and the physical properties of small atoms vis-à-vis bulk metals, need to be tackled.[2-4] Extreme reduction of Pt particles to nanometre scale may significantly change the characteristics of the Pt catalyst and can have favourable or adverse effect to it. Though a conclusive answer to this problem is still lacking, several reports predict that the Pt particle-size of about 3 nm is optimum for improved ORR activity and to reach a maximum mass specific activity.[5-7] Accordingly, strategies for the production of discrete Pt nanoparticles with the desired particle size are of great interest. To address this issue, reducing the size of Pt particles and their deposition on carbon support is favoured.[8,9] Small Pt particle size results in larger surface area available for the chemical reactions and thereby increasing the Pt utilization. However, under harsh conditions, especially at the PEMFC cathode with operating temperature, low pH and high relative humidity, Pt nano particles have a tendency to grow and agglomerate without retaining the electrochemical surface area at higher cycles.[10-13]

In the light of the foregoing, it is therefore required to develop a new catalyst synthesis process wherein (a) precise control of metal particle-size to increase Pt utilization and (b) by preventing the aggregation of Pt nanoparticles to increase stability and durability, will be achieved. To meet these challenges, dendrimers, which are highly branched and three-dimensional macromolecules are useful to control the size, shape and stability of Pt nanoparticles. Dendrimers are well suited for synthesizing metal nanoparticles for the following reasons: (i) uniform composition and structure, which yield a well-defined nanoparticles replicas (ii) metal nanoparticles encapsulated within the dendritic structure prevents agglomeration and growth (iii) nanoparticles are confined primarily by steric effects and therefore prevents the surface passivation (iv) dendrimer branches act as the selective gates to control access of small molecule and (v) the peripheral functional groups of dendrimer control the solubility of encapsulated metal particles and help to anchor on to the solid support.[14]

Dendrimer-encapsulated metal nanoparticles (DENs) are generally prepared by two-step process.[15,16] In the first step, metal ions are inserted into dendrimers where they coordinate with interior functional groups. In the second step, metal-ion/dendrimer composites are reduced to yield encapsulated nanoparticles which are stable and participate in enhancing oxygen reduction reaction (ORR). Crooks et al. studied the immobilisation process of metal encapsulated fourth generation amine group terminated dendrimer (G4-NH_2) onto the support materials.[17-19] In one case, dendrimer surface is partially quaternized in order to increase the number of surface functional groups. The unquaternized primary amine groups left during the process is responsible towards

coupling reaction with the support, while quaternized part will prevent the risk of metal agglomeration. In other case, peripheral amine groups of the dendrimer is selectively protonated, which allow the metal ion interaction with the internal amine groups of the dendrimer. This process provides understanding the protonation steps and its effect on metal ion encapsulation into the dendritic structure.

It is interesting to investigate the interaction of Pt-DENs with carbon and study their ORR behaviour for fuel cell applications. Garcia et al. explained Pt-DENs on carbon as methanol tolerant catalyst where the peculiar dendritic structure inhibits the interference of methanol to Pt nanoparticles which prevents cathode poisoning in direct methanol fuel cells.[20] In our earlier study, Tintula et al. synthesized Pt nanoparticles by encapsulating Pt^{2+} in hydroxyl group terminated fourth generation poly(amidoamine) (G4-OH PAMAM) dendrimer. The resultant DENs were anchored subsequently on to carbon before and after the Pt-reduction process. The Pt-DENs/C catalysts showed improved mass specific activities and the PEMFCs comprising these catalysts on cathode electrodes were performance evaluated with reduced Pt loading (~ 0.125 mg cm^{-2}).[21] The ORR behaviour generally depends on the catalyst size and dispersion which depends on the nature and functionalities of carbon support. For amine terminated dendrimers, the functionalization of carbon is crucial and noteworthy to investigate its interaction with DENs.

The present study provides a facile method for encapsulating Pt nanoparticles in fourth generation amine-terminated poly(amidoamine) dendrimers (G4-NH_2-PAMAM) and their immobilization on to the carbon support. Herein we adopt two different functionalization processes on carbon and studied their effect on immobilisation with Pt-DENs. In method I, carbon is treated with N – hydroxysuccinimide (NHS) which results in the formation of amine reactive semi-stable NHS – ester functional groups on carbon. This further reacts with peripheral amine group for a stable amide linkage between carbon and dendrimer. In method II, carbon reacts with ethyl chloroformate to form active anhydride which further reacts with dendrimer to form amide linkage. The catalysts developed by these methods are physically and electrochemically characterized. The catalyst prepared by anhydride method (method II) exhibits better ORR behaviour with a significant enhancement in mass activity. While evaluating this catalyst in PEMFC, a peak power density of 628 mW cm^{-2} is achieved with cathode catalyst loading 0.2 mg cm^{-2} at 60 °C under ambient pressure.

Experimental section

Materials

Fourth generation amine terminated poly(amidoamine) (G4-NH_2 PAMAM) dendrimer (10 wt % solution in methanol) was purchased from Sigma-Aldrich. Potassium tetrachloroplatinate(II) (K_2PtCl_4), Sodium borohydride ($NaBH_4$), 3-(3-dimethylaminopropyl) 1-Ethyl-carbodiimide (EDC), N-Hydroxysuccinimide (NHS), 2-(N-morpholino) ethanesulfonic acid

(MES) buffer, ethyl chloroformate (ECF, 99%), N-Methylmorpholine (NMM, 99%), Hydrocholoric acid (HCl), Nitric acid (HNO_3), Dimethylformamide (DMF) were procured from Acros Organics. Vulcan XC-72R carbon was obtained from Cabot Corporation. 5 wt % Nafion ionomer was purchased from Du Pont, USA. Milli-Q water (18 MΩ cm) was used to prepare aqueous solution.

Synthesis of dendrimer encapsulated Pt nanoparticles (Pt-DENs)

Pt-DENs were prepared similar to a process reported elsewhere with slight modification.[19,22] Briefly, 200 µL of G4-NH_2 was diluted to 0.05 M by adding DI water. The solution pH was adjusted to 3, 4, 5, 6 and 7 using dilute aqueous HCl. To the above solution, 4 mM aqueous K_2PtCl_4 solution was added and the mixture was stirred continuously for 72 h to allow the Pt^{2+} ions to form complex with interior tertiary amines of dendrimers (G4-NH_2-Pt^{2+}). Zero valent Pt-DENs (G4-NH_2-Pt^0) were obtained by reducing G4-NH_2-Pt^{2+} with 0.3 M aqueous $NaBH_4$ solution under stirring. A reddish brown colour during the reduction process indicates the formation of Pt-DENs. The schematic representation of complexation between Pt^{2+} ions and G4-NH_2-PAMAM dendrimers and their subsequent reduction to metallic Pt are illustrated in Scheme 1.

Functionalization of carbon by NHS ester (C_{est})

Vulcan XC-72R carbon was acid functionalized in conc. HNO_3 under reflux condition for 5 h. The product was washed with distilled water and dried at 80 °C. About 0.15 g of acid functionalized carbon was dispersed in DI water and sonicated for 15 min. To the above dispersion, 100 mL of 0.2 M EDC was added drop-wise in presence of 0.5 M aqueous MES buffer. After 10 min of vigorous stirring, 100 mL of 0.2 M NHS was added and the mixture was further stirred for 1 h for the completion of NHS ester formation reaction. The residue was washed repeatedly with DI water to remove unreacted reagents and dried at 80 °C.[23,24]

Functionalization of carbon by active anhydride (C_{anh})

About 0.15 g of acid functionalized carbon was dispersed in DI water and sonicated for 15 min. The above dispersion was transferred to a beaker containing ECF and NMM dissolved in DMF solution. The admixture was stirred for 1 h in an ice water bath and the temperature was controlled between 0 and 2 °C for the formation of active anhydride on the carbon surface.[25,26] The product was washed thoroughly with DI water and dried at 80 °C.

Immobilization of Pt-DENs on carbon surface

The Pt-DENs immobilization on carbon was done by both ester and anhydride methods. In ester method, C_{est} was dispersed in 20 mL of aqueous 0.5 M MES buffer. The as – prepared Pt-DENs solution was added drop-wise to the above dispersion and stirred for 1 h. Peripheral amine groups of Pt-DENs react with C_{est} to form Pt-DENs/C_{est} composite**.** The obtained Pt-DENs/C_{est}

composite was washed thoroughly with DI water till neutral pH and dried at 50 °C. In anhydride method, C_{anh} was dispersed in 20 mL of DI water and the prepared Pt-DENs was added drop-wise and stirred for 1 h. The residue was filtered and washed with copious amount of DI water and dried at 50 °C. The schematic representation of these two synthesis methods is shown in Scheme 2. Pt/C was prepared by impregnating Pt without dendrimer on Vulcan XC-72R for comparison.

The schematic explanation of dendrimer confined Pt nanoparticles by two different methods mentioned above is shown in scheme 2. This is achieved by a covalent bond between primary amine groups of dendrimer and surface functional groups of carbon. To perform this, initially the carbon surface was functionalized to generate the active functional groups like ester and anhydrides which react with the primary amine functional groups of DENs to form a catalyst. Method I implies the reaction of carbon with EDC/NHS mixture at room temperature to form amine reactive semi-stable NHS ester intermediate (C_{est}). This C_{est} was further treated with Pt-DENs and the primary amines of Pt-DENs react with ester group of carbon to form amide linkage between them. In method II, carbon was treated with ECF and NMM mixture at temperature between 0 and 2 °C to form active anhydride (C_{anh}). Subsequently, primary amines of dendrimers react with anhydride group of carbon and immobilized covalently on carbon by amide bond.

Physicochemical characterization

Complexation process for the samples was monitored at room temperature (25 °C) using UV-visible spectrophotometer (Shimadzu Corporation, Japan) with quartz cuvettes of 1 cm path length. All spectra were background corrected using spectrum obtained from an identical cell filled with de-ionized water and/or aqueous G4-NH_2 solution. The presence of dendrimers on the surface of carbon support was confirmed by Fourier transform infrared (FTIR) spectrophotometer (Thermo Nicolet, Nexus 670). The X-ray diffraction (XRD) patterns were recorded using a Cu Kα source radiation of 1.54 Å in Philips Pan Analytical X-ray diffractometer. The diffractometer was operated in the step scan mode with a 0.02 step at 25 °C. Transmission electron microscope (TEM) images were obtained using a 200 kV Tecnai-20 G2 for analysing Pt dispersion on the catalyst along with particle size and morphology. To identify the electronic features X – Ray photoelectron spectra were recorded by ESCALAB 250 XPS system (Thermo Fisher Scientific) using mono chromated Al Kα source at 15 keV and 150 W system.

Electrochemical characterization

The glassy carbon (GC) disk with area of 0.071 cm^2 was considered as the substrate for working electrode. Pt-DENs/C_{est}, Pt-DENs/C_{anh} and Pt/C catalyst slurries were prepared separately by dispersing 3 mg of each catalyst in 1 mL of DI water with 10 wt % Nafion solution for 30 min under ultra-sonication. To prepare the working electrodes, 5 μL aliquot of the catalyst slurries

were spread on the top of GC electrodes and dried at room temperature. The catalyst loadings of ~30 μg cm^{-2} were obtained on the surface of each working electrode. Electrochemical properties of the catalysts were measured by cyclic voltammogram (CV) and linear sweep voltammogram (LSV) techniques using Autolab PGSTAT 30 (Eco Chemie) at room temperature. A Pt wire and a saturated calomel electrode (SCE) were used as counter and reference electrode, respectively in a standard three-electrode cell. All potentials are reported in terms of the reversible hydrogen electrode (RHE) scale for convenience. Hydrogen adsorption-desorption voltammograms were recorded in 0.1 M aqueous $HClO_4$ solution at a scan rate of 50 mV s^{-1} purging with N_2 gas to remove dissolved O_2. The region for hydrogen adsorption between 0.05 V and 0.4 V vs. RHE on the backward potential scan was used to estimate the electrochemical surface area (ECSA). LSV for ORR measurements was performed in O_2 saturated 0.1 M aqueous $HClO_4$ solution at scan rate of 5 mV s^{-1} with 400, 800, 1200, 1600 and 2000 rotational rates.

Fabrication of membrane electrode assemblies (MEAs) and PEFC performance evaluation

Toray-TGP-H-120 carbon paper of 0.37 mm thickness was used as the backing layer. For the preparation of gas diffusion layer (GDL), Vulcan XC-72R was dispersed in iso-propyl alcohol (IPA) followed by the addition of polytetrafluoroethylene (PTFE) and agitation in an ultrasonic water bath for 30 min. The resultant slurry was coated uniformly onto the backing layer to achieve carbon loading of 1.5 mg cm^{-2}. The obtained GDL was sintered at 350 °C in a furnace for 30 min to get the hydrophobic surface.[27,28] For the catalyst layer, catalysts (Pt-DENs/C_{est}, Pt-DENs/C_{anh} and Pt/C) were dispersed separately in IPA followed by the addition of 30 wt % Nafion with continuous sonication for 30 min. The resultant slurries were coated on to the GDLs (represented as cathodes) until 0.2 mg cm^{-2} of Pt were achieved. For the anode, 20 wt % Pt/C (Johnson Matthey) was used with Pt loading of 0.2 mg cm^{-2}. The MEAs were obtained by sandwiching the pre-treated Nafion 212 membranes between the two electrodes and hot pressed at 130 °C for 3 min under a pressure of 30 kg cm^{-2}.[29] MEAs were coupled with Teflon gas-sealing gaskets and placed in single-cell test fixture with a parallel serpentine flow field machined on graphite plates. H_2 and O_2 gases were fed to the PEMFC anode and cathode respectively, with a flow rate of 200 mL min^{-1} through a bubble humidifier. After equilibration at a cell temperature of 60 °C, galvanostatic polarization data were taken using an LCN100-36 electronic load from Bitrode Corporation, USA. All MEAs were evaluated with an active area of 5 cm^2 in PEFCs under ambient pressure.

Results and discussion

Figure 1a shows UV – vis absorbance spectra for G4 – NH_2 and K_2PtCl_4 complexation reaction with respect to pH. $PtCl_4^{2-}$ ions form complex slowly with interior tertiary amine groups of dendrimer and the optimum pH was found to be 6 where the maximum number of Pt^{2+} ion complexes with the tertiary amines of dendrimers evidenced by the maximum intensity of the absorbance value. Figure 1b shows the absorbance spectra at pH 6 as the function of time. A shoulder peak at about 216 nm corresponds to a ligand-to-metal charge-transfer (LMCT) band of $PtCl_4^{2-}$ due to $5d_z^2 \rightarrow 6p_z$ ($^3a_{1g}$ to $^2a_{2u}$) transition.[30-33] After the

reduction of G4-NH_2-(Pt^{2+}) complex with BH_4- into metallic Pt (G4-NH_2-Pt^0) the shoulder peak at 216 nm decreases and shifts to lower wavelength (210 nm). This peak shift is attributed to the formation of Pt nanoparticles upon borohydride reduction. Further, absorption peak at 260 nm is due to the complexation of Pt^{2+} with tertiary amine groups of the dendrimer through the ligand-to-metal charge-transfer. This absorption intensity increases with time till 72 h. Slow addition of aqueous $NaBH_4$ solution to the G4-NH_2-(Pt^{2+}) complex under agitation results a dark brown coloured G4-NH_2-(Pt^0) due to the reduction of coordinated Pt^{2+} ions in to metallic Pt particles.[19,22] It is also noted that the complexation of Pt^{2+} ions with dendrimers, appears even after reduction, indicates that there are still some unreduced species of Pt^{2+} ions are present. Figure 2a and 2b show the absorbance at 216 nm and 260 nm with respect to reaction time. At pH 6, the maximum absorbance has seen and it is corresponding to the maximum complex formation of $PtCl_4^{2-}$ with dendrimer.

FTIR analysis for C_{est}, C_{anh}, Pt-DENs/C_{est} and Pt-DENs/C_{anh} were performed to find the immobilisation of Pt-DENs to C_{est} and C_{anh} shown in Figure 3. The sharp absorption band at 1640 cm^{-1} is due to the stretching vibrations of C=O group in the ester. The broad peak at 1215 cm^{-1} corresponds to the N-O stretching vibrational frequency in C_{est} indicating the formation of NHS ester on the carbon surface. The two bands at 1730 and 1814 cm^{-1} are due to the stretching vibrations of C=O groups of anhydride in C_{anh} confirm the presence of anhydride group on carbon surface. The vibrational bands around 1630 cm^{-1} and 1550 cm^{-1} are shown in Figure 3c and 3d corresponding to amide I (C=O stretching) and amide II (N-H bending) respectively. These bands confirm that dendrimers are attached covalently by amide linkage on carbon.[34,35]

The XRD patterns for Pt-DENs/C_{est}, Pt-DENs/C_{anh} and Pt/C are shown in Figure 4. The diffraction peaks at 2 theta of 39.8°, 46.2° and 67.4° are assigned to Pt (1 1 1), Pt (2 0 0) and Pt (2 2 0) respectively, shows that all catalysts have Pt in face centered cubic crystal structure.[36] Pt (1 1 1) diffraction peaks are considered to calculate average Pt crystallite sizes for all the catalysts using Debye–Scherrer formula[37], and they are about 3 nm and 3.5 nm for Pt-DENs/C_{est} and Pt-DENs/C_{anh} respectively. The crystallite size of Pt nanoparticles synthesized in the absence of dendrimers is found to be 6.5 nm.

TEM images on the morphologies and distribution of Pt nanoparticles for Pt-DENs/C_{est}, Pt-DENs/C_{anh} and Pt/C catalysts are shown in Figure 5. Pt particles are well dispersed on the carbon support and the average particle sizes of 1.8 and 2.0 nm are observed for Pt-DENs/C_{est} and Pt-DENs/C_{anh} respectively. The dendritic structure prevents growth and agglomeration and thus a uniform distribution of Pt nanoparticles are generated inside the dendrimer cages for both Pt-DENs/C_{est} and Pt-DENs/C_{anh}. Selected area electron diffraction (SAED) patterns shown in the inset to Figure 5a – c confirms the polycrystalline nature of Pt nanoparticles. The diffractions of (1 1 1), (2 0 0) and (2 2 0) lattice planes are consistent with face-centered cubic (fcc) structure of Pt. The broadened SAED rings are due to the smaller particle size of Pt and the corresponding inter – planar spacing of d(1 1 1) = 0.2158, d(2 0 0) = 0.1947 and d(2 2 0) = 0.1391 nm for Pt – DENs/C_{est}. In case of Pt – DENs/C_{anh}, the inter – planar spacing of d(1 1 1) = 0.2074, d(2 0 0) = 0.1843 and d(2 2 0) = 0.1305 nm. In Pt/C, the inter – planar spacing of d(1 1 1) = 0.2217, d(2 0 0)

= 0.1902 and d(2 2 0) = 0.1323 nm and the distances are found to be very close to inter-planar spacing observed for face centred cubic (fcc) structure showing the formation of crystalline Pt nanoparticles[38] The corresponding particle size distribution histograms shown in Figure 5d – f wherein the average particle size distribution for Pt-DENs/C_{est}, Pt-DENs/C_{anh} and Pt/C are 1.8, 2.0 and 4.0 nm in respectively. From the aforesaid, it is noteworthy that the presence of dendrimer helps in controlling the particle size of Pt to a narrow range and is beneficial in increasing the catalyst utilization in the electrochemical oxygen reduction reaction.

To get further insight on the chemical and electronic state of Pt, XPS characterization was carried out and deconvoluted spectra for Pt-DENs/C_{est}, Pt-DENs/C_{anh} are shown in Figure 6. The recorded high resolution scan of Pt (4f) reveals the combination of two pairs of doublets for both Pt-DENs/C_{est} and Pt – DENs/C_{anh} catalysts. The high energy band ($4f_{7/2}$) and low energy band ($4f_{5/3}$) were fitted to their corresponding three peaks. The most intense doublets 71.1 and 74.4 eV (for Pt-DENs/C_{est}); 71.0 and 74.3 eV (for Pt-DENs/C_{anh}) are associated to metallic Pt (Pt^0), and the second set of doublets at binding energy of 72.8 and 76.1 eV (for Pt-DENs/C_{est}); 72.7 and 75.9 eV (for Pt-DENs/C_{anh}) respectively are attributed to Pt^{2+} (PtO or $Pt(OH)_2$). The less intense peaks at 75.2, 78.3 eV (for Pt-DENs/C_{est}); 74.7, 77.8 eV (for Pt-DENs/C_{anh}) endorsed to the presence of Pt in Pt^{4+} state (PtO_2). This indicates that unreduced Pt^{2+} is still found in both the catalyst even after reduction. Similar findings are also observed in the literatures confirms that complete reduction of the Pt is normally not happened during the reduction process.[22] However, similar intensity of Pt^0 found for both the catalysts suggest the equal amount of reduced Pt in Pt-DENs/C_{est} and Pt-DENs/C_{anh} catalysts. Slightly higher binding energies found in Pt-DENs/C_{est} may also be due to lesser particle size of Pt and its interaction to the support during functionalization process.

Cyclic voltammograms of Pt-DENs/C_{est}, Pt-DENs/C_{anh} and Pt/C are shown in Figure 7a. The voltammograms show well defined hydrogen adsorption/desorption peaks between 0.05 V and 0.4 V vs. RHE. A set of anodic and cathodic peaks at 0.6 V and 0.56 V respectively were also observed. These peaks are pseudocapacitive in nature, observed due to the occurrence of oxidation/reduction reactions of the surface functional groups of carbon or may be the adsorption/desorption of anions in the electrolytic solution under acidic conditions. In the present case pseudocapacitive peaks are due to the quinone functionalities (Q) adsorbed on the carbon surface.[39,40] Similar findings are also observed by Andreas et al.[41] and Yu et al.[42] on mesoporous carbon and graphene electrodes in an acidic electrolyte. Electrochemical surface area (ECSA) of Pt of the electrocatalyst was estimated from the equation given below:

$$ECSA = \frac{Q_H}{[Pt] \times 210} \quad (1)$$

where Q_H is the charge of hydrogen desorption on the Pt surface (μC cm^{-2}), [Pt] represents the Pt loading (μg cm^{-2}) and 210 (μC cm^{-2}) represents the charge required to oxidize a monolayer of H_2 on Pt surface of density 1.3×10^{15} atom cm^{-2}.[43] The calculated ECSA values for Pt-DENs/C_{est}, Pt-DENs/C_{anh} and Pt/C are 20.46, 54.8 and 70.12 $m^2\,g^{-1}$ respectively (see Table 1.). ECSA value

for Pt-DENs/C_{anh} is higher in relation to Pt-DENs/C_{est} catalyst which is due to the high reactivity of anhydride functional groups which interact with amine groups of dendrimer to form amide bonds. This further immobilizes large number of dendrimer on to the carbon support (C_{anh}) carrying Pt nanoparticles and thus increases the ECSA. In case of pristine Pt/C, higher ECSA value is obtained may be due to the direct exposure of Pt nanoparticles on the Vulcan carbon which tends to agglomerate during PEFC operation wherein high voltage and acidic environment is prevailed.

The ORR activity behaviour of Pt-DENs/C_{est}, Pt-DENs/C_{anh} and Pt/C are performed by linear sweep voltammograms with sweep rate of 5 mV s^{-1} in O_2 saturated 0.1 M aqueous $HClO_4$ solution shown in Figure 7b. The onset potentials of catalytic current begin at 0.88, 0.92 and 0.91 V for Pt-DENs/C_{est}, Pt-DENs/C_{anh} and Pt/C respectively. The lower onset potential for Pt-DENs/C_{est} attributes to the extreme smaller particle size of Pt which is about 1.8 nm observed from the TEM analysis. It is also reported that extreme miniaturization of Pt particle size greatly varies its electronic and structural properties which in turn affects the ORR activity.[44-46] The decrease in the ORR activity is also due to the adsorption of oxygenated species on to the smaller particles consequently hindering the active sites required for the adsorption of O_2.[47] In addition, the half wave potentials of Pt-DENs/C_{anh} catalyst is positively shifted by 60 mV with respect Pt-DENs/C_{est}, further confirms enhanced ORR kinetics of Pt-DENs/C_{anh} catalyst. The differences in ORR activity may be explained by the variation in the particle size of the two catalysts and their accessible active sites from the morphological orientations.[48] From the foregoing, it is observed that an average of 2 nm Pt particle sized catalyst shows optimum ORR activity in relation to other catalysts studied in this work. For comparison, Pt-DENs was anchored on un-functionalised Vulcan XC-72R and the corresponding CV and LSV were shown in Figure 7a inset. The ECSA of Pt is calculated and found to be 5.4 m^2 g^{-1} which is considerably very less with the catalysts synthesized upon functionalization. The lower onset potential (0.75 V vs. RHE) and half-wave potential (0.51 V vs. RHE) were identified. This reveals that there is no effective immobilisation of Pt-DENs on un-functionalised carbon.

To determine the mass activity (i_m) of the catalysts, the polarization plot for RDE has been corrected for mass-transport by using the following equation.

$$i_k = \frac{i_l i}{i_l - i} \quad (2)$$

where i_k is mass - transport corrected kinetic current density, i_l is the measured limiting current density and i is measured current density. To avoid the risk of inaccuracy of RDE mass-transport corrections at higher current–density values, mass activity for all the catalysts are measured at 0.85 V and evaluated. The i_k values are plotted against the potential which is characteristic of kinetic control region as shown in Figure 7b inset. Extracted electrochemical parameters are presented in Table 1. The mass activities of Pt-DENs/C_{est}, Pt-DENs/C_{anh} and Pt/C are 5.2, 16.4 and 20.5 A g^{-1}_{Pt}, respectively and the specific activities of Pt-DENs/C_{est}, Pt-DENs/C_{anh} and Pt/C are 25.4, 29.9 and 29.2 μA cm^{-2}_{Pt} respectively at 0.85 V (vs. RHE). High specific activity obtained for Pt-

DENs/C_{anh} is due to the greater dispersion of Pt nanoparticles and their interaction with the carbon support. In case of Pt/C, nanoparticles are trapped into the micropores of the support which intend restrict the reactants to access the electrochemical reaction.[21] The present study is the comparison of the electrochemical kinetic behaviours of various catalysts under identical condition. The extremely less particle size of ~ 2 nm in case of dendrimer encapsulated Pt nanoparticles might be the cause in obtaining lower kinetic behaviour. However, optimizing the synthesis process and Pt particle size in order to expose maximum number of Pt particles in ORR and to further increase the kinetic current is the future scope of this study.

Figure 8a, b and c show LSVs of Pt-DENs/C_{est}, Pt-DENs/C_{anh} and Pt/C respectively with different rotational rate (400, 800, 1200, 1600 and 2000 rpm). The corresponding Koutecky-Levich plots are shown in Figure 8d, e and f using the following kinetic equation:

$$\frac{1}{i} = \frac{1}{i_k} + \frac{1}{i_d} \quad (3)$$

$$\frac{1}{i} = \frac{i}{i_k} + \frac{1}{B\omega^{1/2}} \quad (4)$$

where i is measured current density, i_k is kinetic current density, ω is rotation rate, and B is evaluated from the following equation.[49]

$$B = 0.2\, nFAC_{O_2} D_{O_2}^{2/3} \upsilon^{-1/6} \quad (5)$$

where 0.2 is a constant used, n is no. of electron transfer involved in the rate determining step, F is Faraday constant (96,485 C/mol), A is the electrode area (cm^2), C_{O_2} is the concentration of oxygen in electrolyte (1.146×10^{-6} mol cm^{-3}), D_{O_2} is diffusion coefficient of oxygen in the solution (2.17×10^{-5} cm^2 s^{-1}) and υ is kinematic viscosity of $HClO_4$ solution (0.1 m^2 s^{-1}). The linearity and parallelism of K–L plots are correspond to first order reaction kinetics with respect to dissolved O_2 molecule concentration.[50] From K-L plot, the slope value corresponds to the number of electron transfer during ORR calculated to be ~ 3.6 at 0.4 to 0.6 V (vs. RHE) for Pt-DENs/C_{est} (see Figure 8d.). In case of Pt-DENs/C_{anh} and Pt/C the number of electron transfer is found to be ~ 3.8 at 0.4 to 0.6 V (vs. RHE) (see Figure 8e, f.) which is close to 4 revealing that the ORR proceeds through a four electron transfer process wherein the H_2O is formed as the product. In DENs the dendritic structure provides a high degree of control over Pt particle size and dispersity. Besides, dendrimer itself has the catalytic active sites which help in the reaction.

In order to validate these catalysts for PEFC application, MEAs are configured by employing these catalysts at the cathode of fuel cell. The PEFC polarization and power density data in H_2-O_2 cell at 60 °C and ambient pressure is shown in Figure 9. It is noteworthy, that the peak power densities of 628 mW cm^{-2} and 502 mW cm^{-2} are achieved for PEFC with catalysts comprising of

Pt-DENs/C_{anh} and Pt-DENs/C_{est} respectively with the catalyst loading of 0.2 mg cm^{-2}. However, the peak power density of 586 mW cm^{-2} is obtained for Pt/C without dendrimer. The improved performance in the MEA comprising Pt-DENs/C_{anh} as the cathode catalyst adds the superior attention from the other. It is noteworthy, that the overall ORR behaviour for the dendrimer confined nanoparticles may be slightly less, but the acidic fuel cell environment protonates the amide groups of the dendrimer and improves ionic conduction which is beneficial in improving three phase contact on PEFC electrodes. As a result, improved power density is achieved for Pt/DENs catalyst synthesized through anhydride method. Although the catalytic reaction within dendrimer structure is not well understood and it is evidently inferred that dendrimer provides great control of identical nanoparticles which enhance the distribution of the active phase on the electrode material which improve the PEFC performance.

Conclusions

Pt nanoparticles prepared within amine-terminated PAMAM dendrimers by selective protonation of primary amine groups and metal-ion complexation with tertiary amine groups. The pH and reaction time at which the maximum metal complexation occurs during the synthesis was optimized using UV-vis spectrophotometer. Pt-DENs was successfully immobilized on NHS-ester functionalized carbon and mixed anhydride functionalized carbon. Nanoparticles are distributed uniformly on the carbon support with a particle size of ≤ 2.5 nm. Pt-DENs supported carbon through anhydride route gives the better activity than the catalyst synthesized through ester method. The use of G4-NH_2 PAMAM dendrimer provides size-controlled preparation of the Pt based catalysts with uniform dispersion and loading of the catalysts onto carbon supports with increased PEFC performance.

Acknowledgements

The authors acknowledge CSIR, New Delhi, for financial support through HYDEN (CSC – 0122). We thank Dr. V. V. Giridhar, Scientist-in-Charge, CECRI Madras unit, and Dr. Vijayamohanan K. Pillai, Director, CECRI, Karaikudi, for their constant encouragement and support. We also thank Ms. S. Meenakshi for her motivation. The authors acknowledge Mr. A. Rathish Kumar, Central Instrument Facility, Karaikudi, for his help in TEM analysis.

Notes and references

CSIR-Central Electrochemical Research Institute - Madras unit, CSIR Madras Complex, Taramani, Chennai - 600 113, INDIA

*E-mail: aksahu@cecri.res.in
Telephone: +91- 44-22544554.

1 H. A. Gasteiger, S. S. Kocha, B. Sompalli and F. T. Wagner, *Appl. Catal. B: Environ.*, 2005, **56**, 9.

2 Y. Sun, L. Zhuang, J. Lu, X. Hong and P. Liu, *J. Am. Chem. Soc.*,2007, **129**, 15465.

3 C. Aslhart and E. Uggerud, *Chem. Commun.*, 2006, 2581.

4 G. N. Vayssilov, Y. Lykhach, A. Migani, T. Staudt, G. P. Petrova, N. Tsud, T. Skála, A. Bruix, F. Illas, K. C. Prince, V. Matolı´n, K. M. Neyman and J. Libuda, *Nat. Mater.*, 2011, **10**, 310.

5 Y. Verde, G. Alonso-Nunez, M. Miki-Yoshida, M. Jose-Yacaman, V. H. Ramos and A. Keer, *Catal. Today*, 2005, **107**, 826.

6 F. Raimondi, G. G. Scherer, R. Koz and A. Wokaun, *Angew. Chem. Int. Ed.*, 2005, **44**, 2190.

7 P. J. Ferreira, G. J. la O', Y. Shao-Horn, D. Morgan, R. Makharia, S. Kocha and H. A. Gasteiger, *J. Electrochem. Soc.*, 2005, **152**, A2256.

8 S. Song, Y. Liang, Z. Li, Y. Wang, R. Fu, D. Wu and P. Tsiakaras, *Appl. Catal. B: Environ.,* 2010, **98**, 132.

9 M. S. Wilson, F. H.Garzon, K. E.Sickafus and S.Gottesfeld, *J. Electrochem. Soc.*, 1993, **140**, 2872.

10 J. Xie, D. L. Wood, D. M. Wayne, T. A. Zawodzinski, P. Atanassov and R. L. Borup, *J. Electrochem. Soc.*, 2005, **152**, A104.

11 S. Y. Huang, P. Ganesan and B. N. Popov, *Appl. Catal. B: Environ.*, 2011, **102**, 71.

12 Y. Y. Shao, G. P. Yin and Y. Z. Gao, *J. Power Sources*, 2007, **171**, 558.

13 Z. Xu, H. Zhang, H. Zhong, Q. Lu, Y. Wang and D. Su, *Appl. Catal. B: Environ.*, 2012, **111**, 264.

14 R. M. Crooks, M. Zhao, L. Sun, V. Chechik and L. K. Yeung, *Acc. Chem. Res.*, 2001, **34**, 181.

15 R. W. J. Scott, O. M. Wilson and R. M. Crooks, *J. Phys. Chem. B*, 2005, **109**, 692.

16 H. Ye and R. M. Crooks, *J. Am. Chem. Soc.*, 2005, **127**, 4930.

17 S. K. Oh, Y. G. Kim, H. Ye and R. M. Crooks, *Langmuir*, 2003, **19**, 10420.

18 V. Chechik, M. Zhao and R. M. Crooks, *J. Am. Chem. Soc*., 1999, **121**, 4910.

19 H. Ye, R. W. J. Scott and R. M. Crooks, *Langmuir*, 2004, **20**, 2915.

20 J. L. Garcia, I. L. E. Garcia, T. W. Chapman, L. G. Arriaga, V. Baglio, V. Antonucci, A. S. Arico, R. Ornelas and L. A. Godinez, *J. Solid State Electrochem.*, 2010, **14**, 835.

21 K. K. Tintula, A. K. Sahu, S. D. Bhat, S. Pitchumani and P. Sridhar, *Appl. Catal. B: Environ.*, 2011, **110**, 178.

22 M. Zhao and R. M. Crooks, *Adv. Mater.*, 1999, **11**, 217.

23 C. Wang, Q. Yan, H. B. Liu, X. H. Zhou, and S. J. Xiao, *Langmuir*, 2011, **27**, 12058.

24 S. Sam, L. Touahir, J. S. Andresa, P. Allongue, J. N. Chazalviel, A. Laemmel, C. H. de Villeneuve, A. Moraillon, F. Ozanam, N. Gabouze and S. Djebbar, *Langmuir*, 2010, **26**, 809.

25 M. L. Bruening, Y. Zhou, G. Aguilar, R. Agee, D. E. Bergbreiter and R. M. Crooks, *Langmuir*, 1997, **13**, 770.

26 D. E. Bergbreiter and G. Tao, *J. Polym. Sci., Part A: Polym. Chem.,* 2000, **38**, 3944.

27 G. Selvarani, S. Vinod Selvaganesh, S. Krishnamurthy, G. V. M. Kiruthika, P. Sridhar, S. Pitchumani and A. K. Shukla, *J. Phys. Chem. C*, 2009, **113**, 7461.

28 A. K. Sahu, K. G. Nishanth, G. Selvarani, P. Sridhar, S. Pitchumani and A. K. Shukla, *Carbon*, 2009, **47**, 102.

29 S. Gouse Peera, K. K. Tintula, A. K. Sahu, S. Shanmugam, P. Sridhar and S. Pitchumani, *Electrochimica Acta*, 2013, **108**, 95.

30 D. Yamamoto, S. Watanabe and M. T. Miyahara, *Langmuir*, 2010, **26**, 2339.

31 L. I. Elding and L. F. Olsson, *J. phy chem.*, 1978, **82**, 69.

32 J. Chatt, G. A. Gamlen and L. E. Orgel, *J. Chem. Soc.*, 1958, 486.

33 D. Yamamoto, S. Watanabe and M. T. Miyahara, *Ind. Eng. Chem. Res.*, 2011, **50**, 7332.

34 M. Wells and R. M. Crooks, *J. Am. Chem. Soc.*, 1996, **118**, 3988.

35 H. Tokuhisa, M. Zhao, L. A. Baker, V. T. Phan, D. L. Dermody, M. E. Garcia, R. F. Peez, R. M. Crooks and T. M. Mayer, *J. Am. Chem. Soc.*, 1998, **120**, 4492.

36 C. He, H. R. Kunz and J. M. Fenton, *J. Electrochem. Soc.,* 144, 1997, 970.

37 A. Pozio, M. D. Francesco, A. Cemmi, F Cardellini and L. Giorgi, *Journal of Power Sources,* 2002, 105, 13.

38 T. K. Zvonareva, A. A. Sitnikova, G. S. Frolova and V. I. I. Omskiĭ, *Semiconductors*, 2008, **42**, 325.

39 H. P. Boehm, *Carbon*, 1994, **32**, 759.

40 P. Bentley, D. A. Stone and N. Schofield, *J. Power Sources*, 2005, **147**, 288.

41 H. A. Andreas and B. E. Conway, *Electrochim. Acta*, 2006, **51**, 6510.

42 H. Yu, J. He, L. Sun, S. Tanaka and B. Fugetsu, *Carbon*, 2013, **51**, 94.

43 G. Faubert, D. Guay and J. P. Dodelet, *J. Electrochem. Soc.*, 1998, **145**, 2985.

44 M. Peuckert, T. Yoneda, R. A. D. Betta and M. Boudart, *J. Electrochem. Soc.*, 1986, **133**, 944.

45 V. Raghuveer, A. Manthiram and A. J. Bard, *J. Phys. Chem. B*, 2005, **109**, 22909.

46 M. H. Shao, K. Sasaki and R. R. Adzic, *J. Am. Chem. Soc.*, 2006, **128**, 3526.

47 K. J. J. Mayrhofer, B. B. Blizanac, M. Arenz, V. R. Stamenkovic, P. N. Ross and N. M. Markovic, *J. Phys. Chem. B*, 2005, **109**, 14433.

48 H. Ye, J. A. Crooks and R. M. Crooks, *Langmuir*, 2007, **23**, 11901.

49 N. Wkabayashi, M. Takeichi, M. Itagaki, H. Uchida and M. Watanabe, *J. Electroanal. Chem.*, 2005, **574**, 339.

50 J. N. Tiwari, K. Nath, S. Kumar, R. N. Tiwari, K. C. Kemp, N. H. Le, D. H. Youn, J. S. Lee and K. S. Kim, *Nat. Commun.*, 2013, **4**, doi:10.1038/ncomms3221.

Figure captions

Figure 1. Time-resolved UV-vis absorbance spectra for G4-NH_2 and Pt^{2+}complexation reaction (a) absorbance as a function of pH at 72 h, (b) absorbance as a function of time (up to 72 h) and after reduction with $NaBH_4$ at pH 6.

Figure 2. Plots for (a) absorbance at λ = 216 nm for $PtCl_4^{2-}$ and (b) absorbance at λ = 260 nm for the G4-NH_2-(Pt^{2+}) complexes as a function of time at pH 6.

Figure 3. FTIR spectra of (a) C_{est}, (b) C_{anh}, (c) Pt – DENs/C_{est} and (d) Pt – DENs/C_{anh} at 25 °C.

Figure 4. Comparative XRD pattern of Pt-DENs/C_{est}, Pt-DENs/C_{anh} and Pt/C catalysts at 25 °C.

Figure 5. TEM images of (a) Pt-DENs/C_{est}, (b) Pt-DENs/C_{anh}, (c) Pt/C catalysts, (d), (e) and (f) are the average particle size and distribution curves of Pt-DENs/C_{est}, Pt-DENs/C_{anh} and Pt/C respectively. The insets are the corresponding selective area electron diffraction.

Figure 6. X – Ray photoelectron spectra of the Pt (4f) region for (a) Pt-DENs/C_{est} and (b) Pt-DENs/C_{anh}.

Figure 7. (a) Cyclic voltammograms of Pt-DENs/C_{est}, Pt-DENs/C_{anh} and Pt/C catalysts modified GCEs in the potential range between 0 – 1.2 V (vs. RHE) in N_2 saturated 0.1 M aqueous $HClO_4$ at a scan rate of 50 mV s^{-1}. Inset represents CV and LSV of Pt-DENs anchored on un-functionalised Vulcan XC-72R modified GCE. (b) Linear sweep voltammograms of Pt-DENs/C_{est}, Pt-DENs/C_{anh} and Pt/C catalysts in O_2 saturated 0.1 M aqueous $HClO_4$ at a scan rate of 5 mV s^{-1} with rotation rate of 1600 rpm. The inset represents mass-transfer-corrected Tafel plots (i_k vs. V (vs. RHE)). The electrode preparation is discussed in the corresponding section. The geometric area of the GCE is 0.071 cm^2. All the voltammograms were recorded at 25 °C.

Figure 8. Rotating disk voltammograms of (a) Pt-DENs/C_{est}, (b) Pt-DENs/C_{anh} and (c) Pt/C modified GCEs. The scan rate was 5 mV s^{-1} with different rotational rate in 0.1 M aqueous $HClO_4$ solution at 25 °C. (d), (e) and (f) are Koutecky-Levich plots of Pt-DENs/C_{est}, Pt-DENs/C_{anh} and Pt/C respectively.

Figure 9. Comparison of Pt-DENs/C_{est}, Pt-DENs/C_{anh} and Pt/C catalysts cell polarization and power density curves for H_2-O_2 fuel cells operated at 60 °C and 200 mL min^{-1} fuel flow controlled by the mass flow controller. 0.2 mg cm^{-2} Pt loading on the cathode side of Pt-DENs/C_{est}, Pt-DENs/C_{anh} and Pt/C modified MEAs. 20 wt % commercial Pt/C was used at the anodic catalyst of 0.2 mg $cm^{-2}{}_{Pt}$.

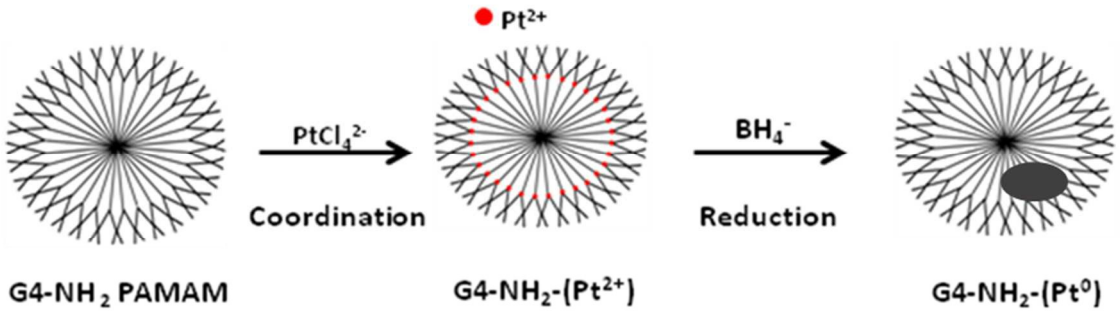

Scheme 1. Schematic illustration of complexation and reduction process of G4-NH_2 – PAMAM dendrimers and K_2PtCl_4.

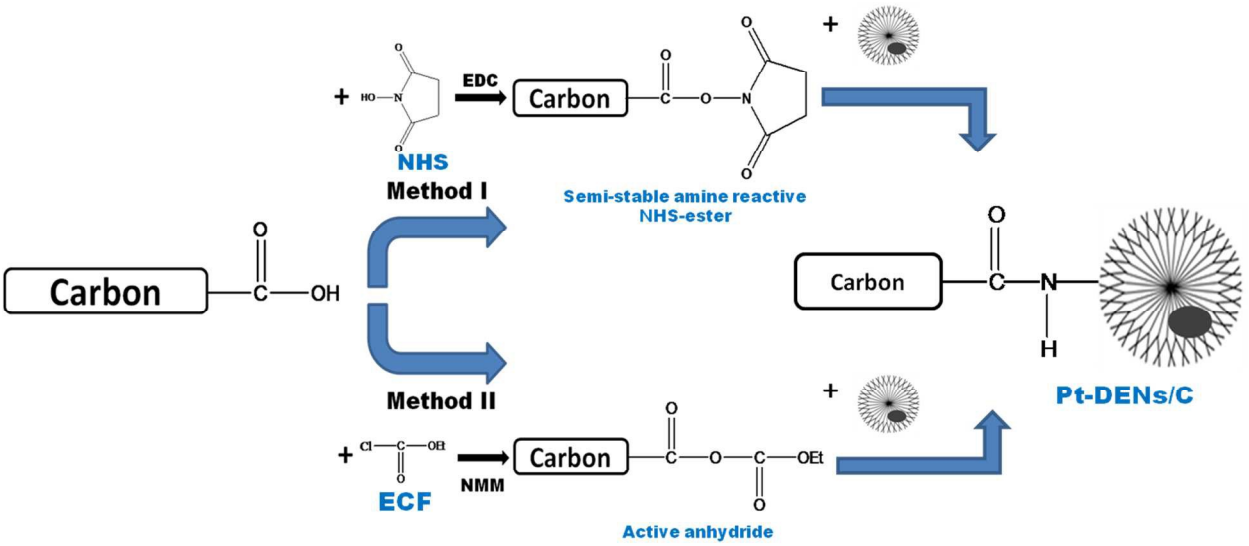

Scheme 2. Schematic illustration of immobilization of Pt-DENs onto ester functionalized carbon and active anhydride functionalized carbon.

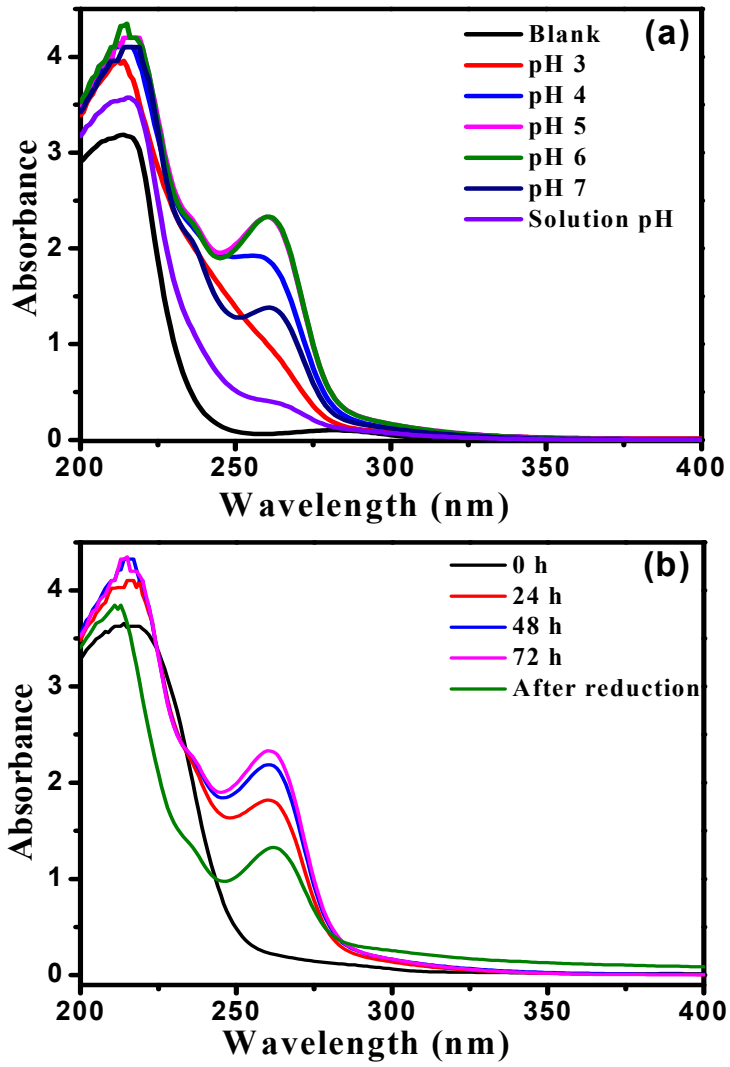

Figure 1. Time-resolved UV-vis absorbance spectra for G4-NH_2 and Pt^{2+}complexation reaction (a) absorbance as a function of pH at 72 h, (b) absorbance as a function of time (up to 72 h) and after reduction with $NaBH_4$ at pH 6.

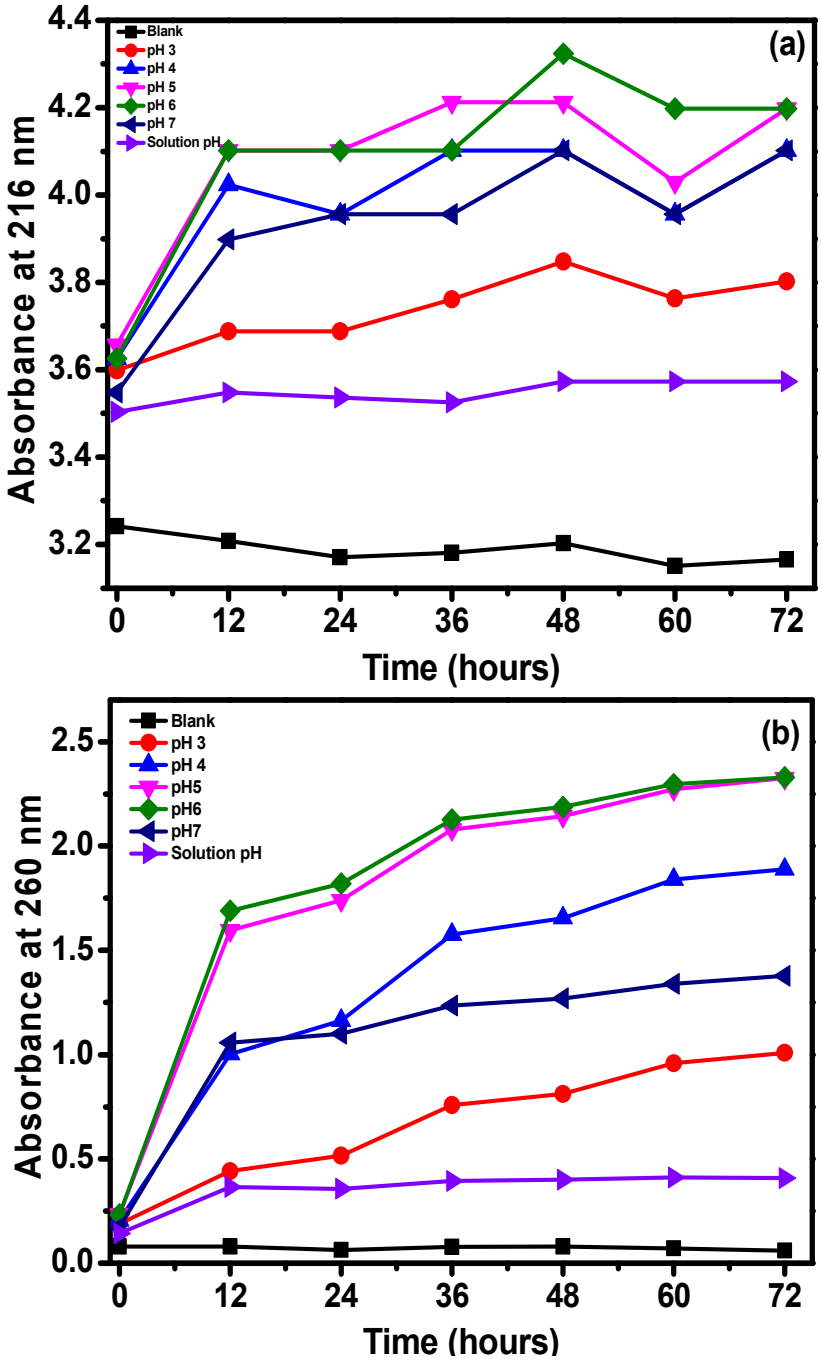

Figure 2. Plots for (a) absorbance at λ = 216 nm for $PtCl_4^{2-}$ and (b) absorbance at λ = 260 nm for the G4-NH_2-(Pt^{2+}) complexes as a function of time at pH 6.

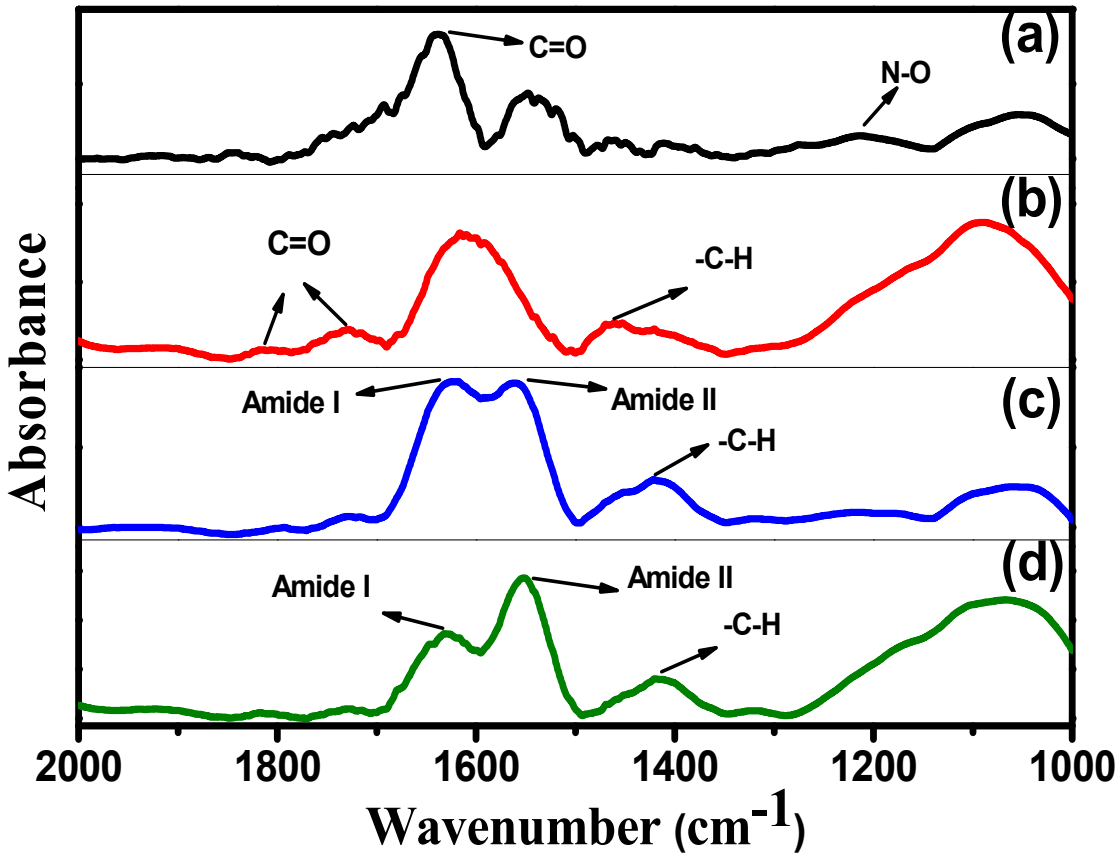

Figure 3. FTIR spectra of (a) C_{est}, (b) C_{anh}, (c) Pt – DENs/C_{est} and (d) Pt – DENs/C_{anh} at 25 °C.

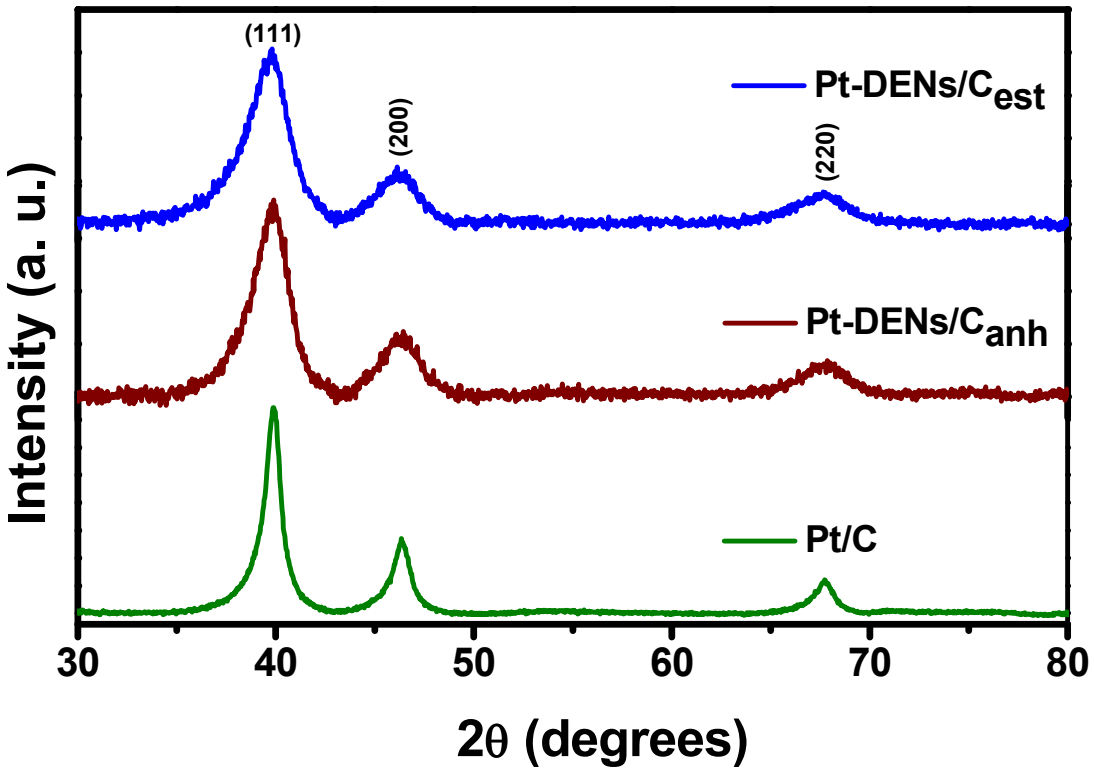

Figure 4. Comparative XRD pattern of Pt-DENs/C_{est}, Pt-DENs/C_{anh} and Pt/C catalysts at 25 °C.

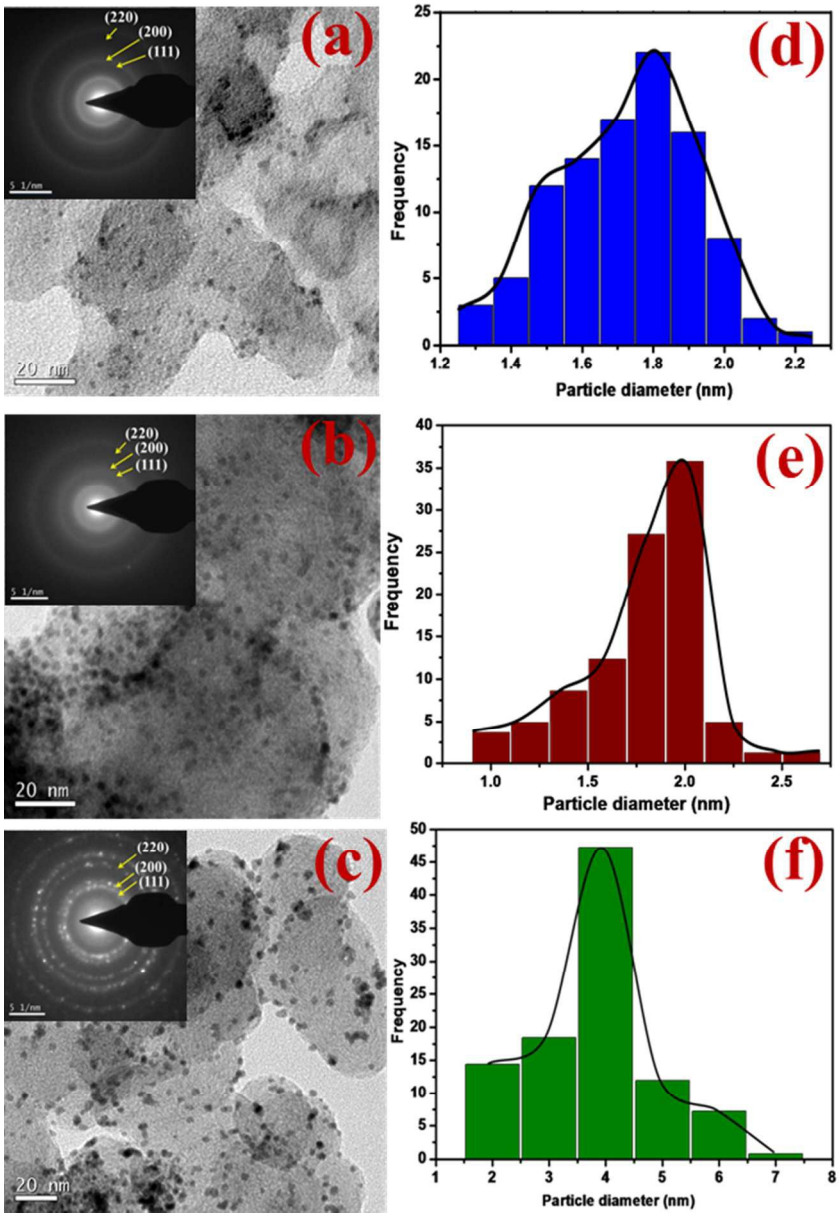

Figure 5. TEM images of (a) Pt-DENs/C_{est}, (b) Pt-DENs/C_{anh}, (c) Pt/C catalysts, (d), (e) and (f) are the average particle size and distribution curves of Pt-DENs/C_{est}, Pt-DENs/C_{anh} and Pt/C respectively. The insets are the corresponding selective area electron diffraction patterns.

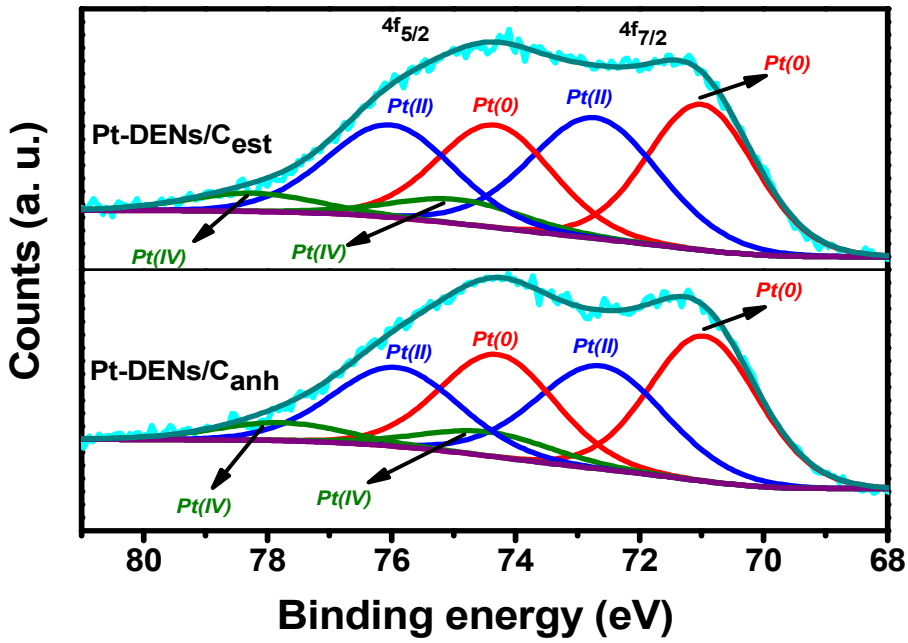

Figure 6. X – Ray photoelectron spectra of the Pt (4f) region for (a) Pt-DENs/C_{est} and (b) Pt-DENs/C_{anh}.

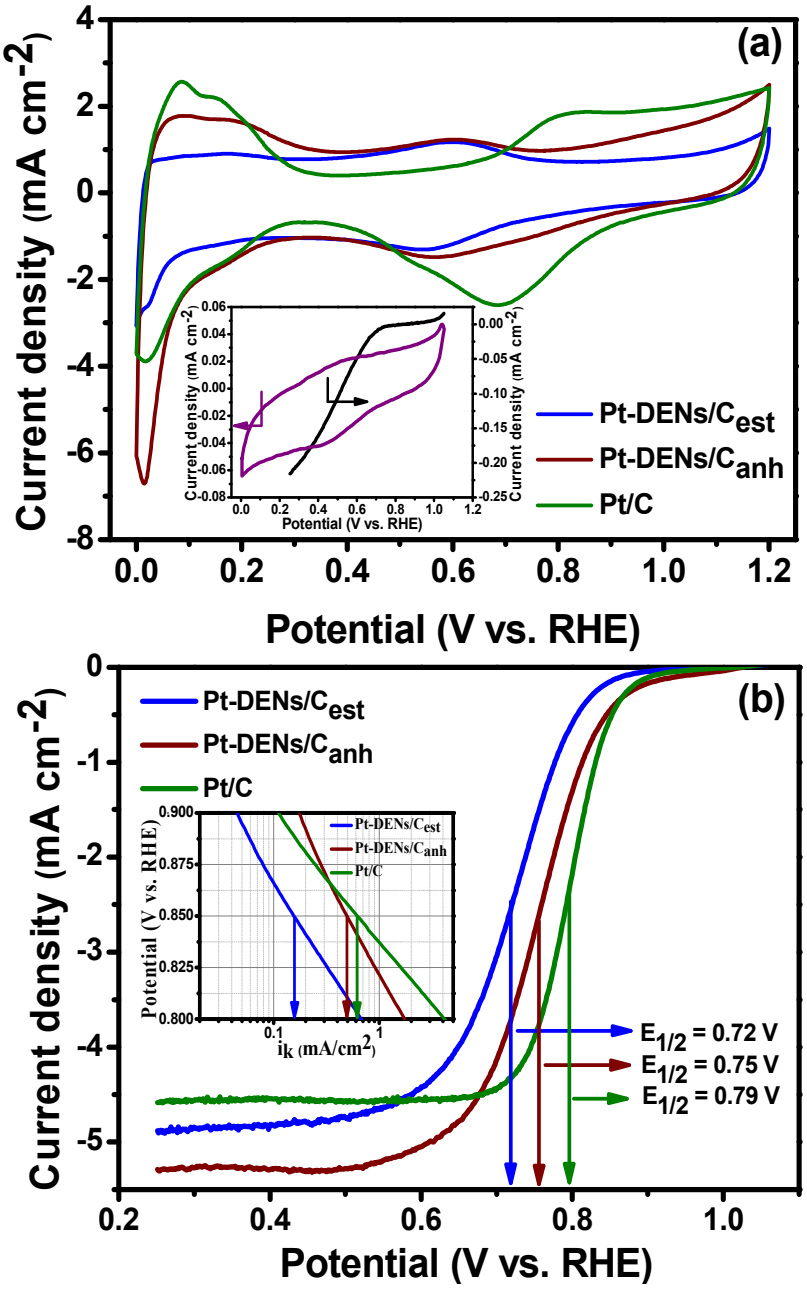

Figure 7. (a) Cyclic voltammograms of Pt-DENs/C_{est}, Pt-DENs/C_{anh} and Pt/C catalysts modified GCEs in the potential range between 0 – 1.2 V (vs. RHE) in N_2 saturated 0.1 M aqueous $HClO_4$ at a scan rate of 50 mV s^{-1}. Inset represents CV and LSV of Pt-DENs anchored on un-functionalised Vulcan XC-72R modified GCE. (b) Linear sweep voltammograms of Pt-DENs/C_{est}, Pt-DENs/C_{anh} and Pt/C catalysts in O_2 saturated 0.1 M aqueous $HClO_4$ at a scan rate of 5 mV s^{-1} with rotation rate of 1600 rpm. The inset represents mass-transfer-corrected Tafel plots (i_k vs. V (vs. RHE)). The electrode preparation is discussed in the corresponding section. The geometric area of the GCE is 0.071 cm^2. All the voltammograms were recorded at 25 °C.

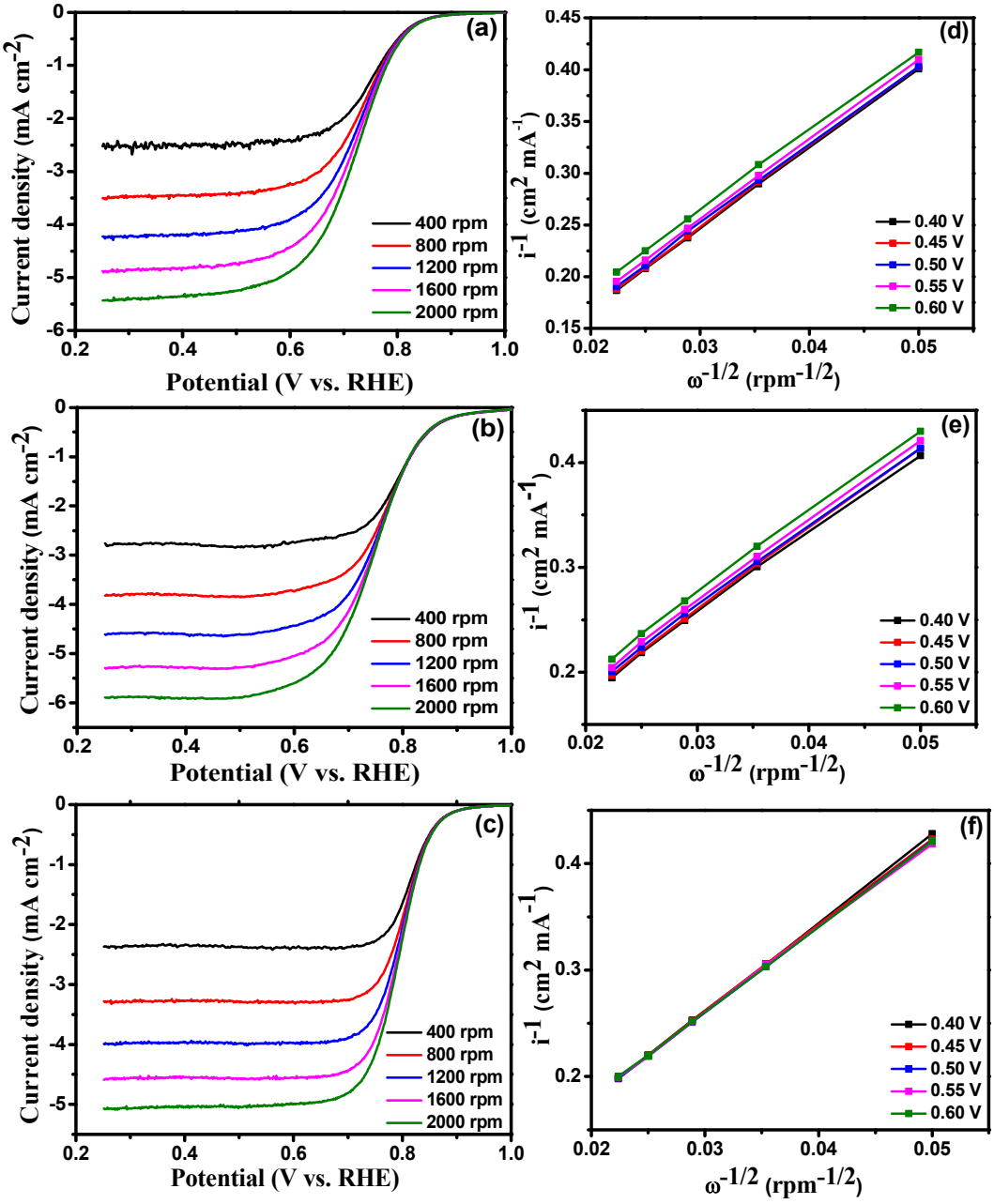

Figure 8. Rotating disk voltammograms of (a) Pt-DENs/C_{est}, (b) Pt-DENs/C_{anh} and (c) Pt/C modified GCEs. The scan rate was 5 mV s^{-1} with different rotational rate in 0.1 M aqueous $HClO_4$ solution at 25 °C. (d), (e) and (f) are Koutecky-Levich plots of Pt-DENs/C_{est}, Pt-DENs/C_{anh} and Pt/C respectively.

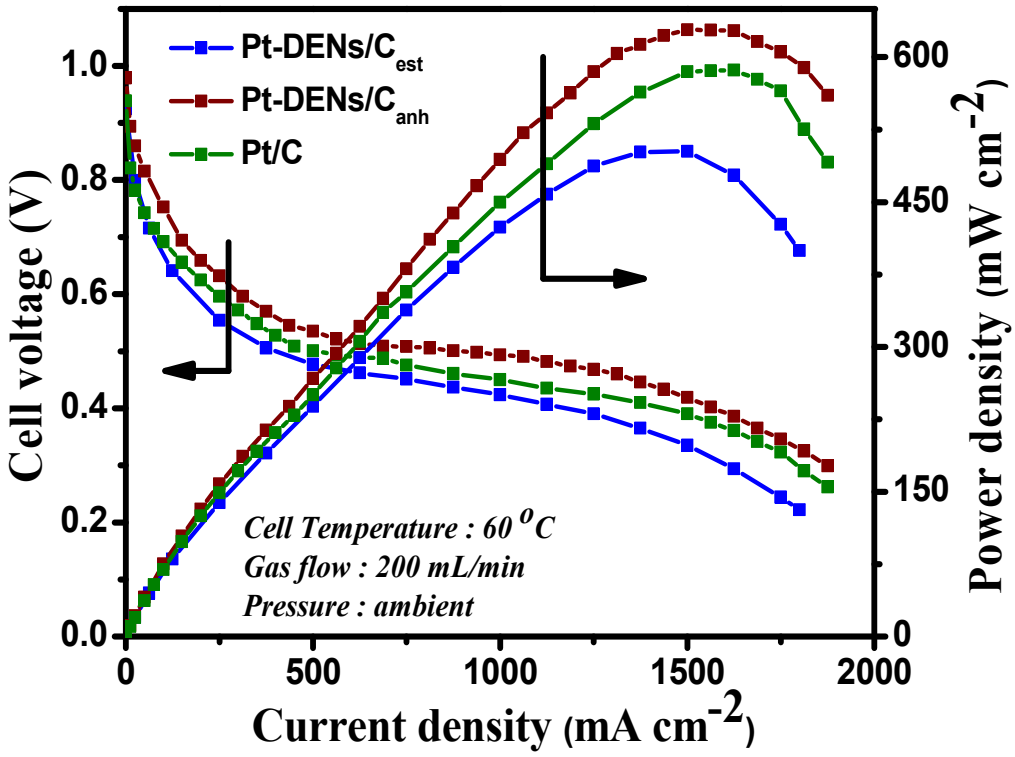

Figure 9. Comparison of Pt-DENs/C_{est}, Pt-DENs/C_{anh} and Pt/C catalysts cell polarization and power density curves for H_2-O_2 fuel cells operated at 60 °C and 200mL min^{-1} fuel flow controlled by the mass flow controller. 0.2 mg cm^{-2} Pt loading on the cathode side of Pt-DENs/C_{est}, Pt-DENs/C_{anh} and Pt/C modified MEAs. 20 wt % commercial Pt/C was used at the anodic catalyst of 0.2 mg $cm^{-2}{}_{Pt}$.

Table 1. Comparison of ECSA, kinetic current (i_k), mass activities (i_m) and specific activities (i_s) for ORR at 0.85 V vs. RHE determined at a rotation rate of 1600 rpm and scan rate of 5 mV s^{-1} at 25 °C.

Catalysts	**ECSA (m^2/g)**	**i_k (μA)**	**i_m (A/g_{Pt})**	**i_s ($\mu A/cm^2_{Pt}$)**
Pt-DENs/C_{est}	20.46	11.0	5.2	25.4
Pt-DENs/C_{anh}	54.80	34.9	16.4	29.9
Pt/C	70.12	43.8	20.5	29.2